International Forum on Aeroelasticity and Structural Dynamics
IFASD 2024
17-21 June 2024, The Hague, The Netherlands

PREDICTION OF LIMIT CYCLE OSCILLATIONS BASED ON DYNAMIC EIGEN DECOMPOSITION OF FLIGHT TEST DATA

John (Taehyoun) Kim
tkim07@uw.edu
Department of Mechanical Engineering
University of Washington, Bothell, WA, USA

Keywords: Limit cycle oscillation (LCO), LCO prediction, freeplay, control surface, dynamic eigenmodes, dynamic eigen decomposition, flutter prediction, flight flutter test (FFT).

Abstract: During design and analysis phases of aircraft flutter boundaries are computed using analysis tools such as the p-k iterations or eigenvalue analysis. Also, for the purpose of certification flight flutter test (FFT) is conducted to predict the onset of flutter experimentally. However, from the practical perspective aeroelastic vibrations with finite amplitudes known as the Limit Cycle Oscillation (LCO) are more critical because they reveal the true nonlinear nature of the fluid-structure interaction. Previously, based on the concept of the Dynamic Eigen Decomposition (DED) and a frequency domain stability theorem, a new flutter prediction methodology was developed for applications to FFT with limited actuators and sensors. In this study, this technique is extended to include LCOs originating from a nonlinearity existing in a control surface freeplay. First, a linear flutter boundary is predicted using the DED method and data available at subcritical flight conditions. Next, a simple harmonic analysis of the control surface freeplay is carried out to extract important harmonic contents of the nonlinearity, and a new DED is formulated in two parameters, i.e., the variable dynamic pressure and the effective stiffness of the control surface hinge. Using the formulation, it is possible to predict LCO by extrapolating the dynamic eigenvalues obtained at the subcritical data points. The proposed methodology is demonstrated using computational simulations of a tapered wing with four flaps and a freeplay in one of the hinges. It is shown that the new approach yields accurate predictions of LCO without need for taking additional data, with only the data obtained during the FFT.

1 INTRODUCTION

Flutter is a well-known mechanism by which air vehicles become dynamically unstable through the interaction of the fluid forces and elastic deformation of the structure. It is a dangerous phenomenon to be avoided during the design, analysis, and tests of all airplanes. Although there exist analyses and tools that enable estimating the onset of aeroelastic instability, they are often subject to modeling errors, uncertainties, and limitations that can produce inaccurate, unreliable results. On the other hand, flight test data are a direct reflection of the actual aircraft and therefore they are usually accepted with good credibility. Today, it is a customary practice and requirement in the aeronautical industry to conduct flight flutter tests before the aircraft enters its service.

There exist excellent literature surveys that discuss various flutter prediction methods based upon subcritical (below the flutter boundary) data [1-2]. They include Damping Extrapolation,

Envelope Function, Zimmerman-Weissenburger, Discrete-Time Autoregressive Moving Average (ARMA), Flutterometer, and the Nissim and Gilyard method [3-8]. The first two methods introduce stability parameters that are valid only at a specific dynamic pressure under consideration, and hence they heavily depend on extrapolation of the information to higher speeds. The other methods consider a coupled fluid-structure system with a variable dynamic pressure. The Zimmerman-Weissenburger [5] utilizes the coupled equations of motion, applies the Routh stability criterion using a quadratic stability parameter, and solves for the flutter margin. However, its application is limited to two degrees of freedom classical bending torsion flutter with quasi-steady aerodynamics. The Flutterometer [7] is based on an analytical flutter model rather than the test data. To account for possible uncertainties and modeling errors in the analysis, certain parts of the model are updated analytically. The result is a robust aeroelastic stability formulation. Unfortunately, its flutter margin solution is known to be too conservative to be realistic. Nissim et al [8] developed a frequency domain system identification scheme in which the aerodynamic and structural properties are extracted by manipulating frequency responses of the airplane at two different dynamic pressures. But a quasi-steady assumption of the unsteady aerodynamics must be made to minimize the number of unknowns. Another work worth mentioning is that of Song et al [9] in which the AAEMS (Aerodynamics is Aeroelasticity Minu Structure) developed by Kim [10] was used to search for onset of flutter of a rigid wing specimen in a low-speed wind tunnel. Despite the absence of aerodynamic measurements, their results were encouraging in that the system identification could still lead to a reliable flutter prediction provided the data is taken at a speed not too far from the flutter speed. Recently, Roizner et al [11] introduced the Parametric Flutter Margin (PFM) method in which a control system is added to the aeroelastic system to take it beyond its nominal flutter point. Then by testing the controlled stable system at the nominal flutter point, one can infer the nominal flutter point using Nyquist type criteria. Besides obtaining the flutter margin, it has the advantage of treating linear and nonlinear flutter by the unified approach.

All of these flutter testing methods have a common and serious issue that they will produce converged results only if the data being used has been collected near the flutter point. That is, none of them fully accounts for the fundamental aspects of FSI (Fluid-Structure Interaction). As a remedy for this drawback, Kim recently introduced the new concept of the Dynamic Eigenmodes and Decomposition and applied it successfully to flutter prediction showing that the prediction can be done accurately at any flight speeds and altitudes [12-15]. In particular, he showed that the new approach can take advantage of the present-day practice, i.e., a progressive flutter testing such that test data due to multiple inputs can be replaced by test data due to limited inputs obtained at multiple flight points [15].

Moving to LCO prediction, literature is sparse due to technical challenges to be overcome to make measurement of large amplitudes feasible. There has been a fair number of works in computational simulations, analyses, and wind tunnel testing of LCO [16-19], but little has been done to establish an experimental methodology to predict the nonlinear phenomenon.

In the present work, the original flutter prediction scheme developed for theory and experimental testing based on the DED [14-15] is modified and extended to account for large amplitude LCOs. For this initial work, we focus on structural nonlinearity caused by a control surface freeplay, assuming that aerodynamically the system remains statically nonlinear but dynamically linearized. As in the linear flutter prediction, the LCO can be interpreted as a dynamic instability with a zero

effective damping if the nonlinear solution is approximated in a simple harmonic fashion, similar to the harmonic balance approach to general engineering problems. Thus, as in the linear flutter prediction an LCO can be determined by checking the dynamic eigenvalues in the frequency domain with an effective control surface stiffness. In particular, it is shown that the LCO which stems from the control surface freeplay can be traced using only one actuator and one sensor attached on the control surface. Furthermore, the LCO mode is just the forced response due to the single degree-of-freedom control surface excitation. These are very promising outcomes of the new formulation as it bodes well for LCO prediction based on flight test data. The proposed scheme is demonstrated using a tapered straight wing with four flaps. Linear flutter is first obtained using the previous method [15]. Then, LCO solutions are sought allowing variation in the control surface stiffness as well as dynamic pressure. It is shown that the new approach can yield accurate predictions of LCO without taking additional tests, with only the data obtained from the FFT.

2 DYNAMIC EIGEN DECOMPOSITION OF AEROELASTIC SYSTEM

In this section, the DED used for the aforementioned flutter prediction method [14] is reviewed.

The aeroelastic formulation is derived conveniently using the coupled aeroelastic equations of motion using the generalized modal coordinates $\boldsymbol{q}$ in the mixed time/frequency domain:

$$\boldsymbol{M}\ddot{\boldsymbol{q}} + \boldsymbol{C}\dot{\boldsymbol{q}} + \boldsymbol{K}\boldsymbol{q} = q_D\boldsymbol{Q}(M_\infty, k)\boldsymbol{q} \quad (N \times 1) \tag{1}$$

If we fix Mach number under the mild assumption that the speed of sound does not change with altitude the only parameter that varies is dynamic pressure, q_D [14]. Following the so called the Constant Mach Varying Altitude (CMVA) approach, we divide the solution into the nominal and perturbed parts as $\boldsymbol{q} = \boldsymbol{q}_0 + \boldsymbol{\Delta q}$, with the nominal $\boldsymbol{q}_0$ denoting the reference dynamic pressure q_{D_0}, leads to

$$\boldsymbol{M}\ddot{\boldsymbol{q}}_0 + \boldsymbol{C}\dot{\boldsymbol{q}}_0 + \boldsymbol{K}\boldsymbol{q}_0 - q_{D_0}\boldsymbol{Q}(k)\boldsymbol{q}_0 = \boldsymbol{0} \tag{2}$$

$$\boldsymbol{M}\boldsymbol{\Delta}\ddot{\boldsymbol{q}} + \boldsymbol{C}\boldsymbol{\Delta}\dot{\boldsymbol{q}} + \boldsymbol{K}\boldsymbol{\Delta q} - q_D\boldsymbol{Q}(k)\boldsymbol{\Delta q} - \Delta q_D\boldsymbol{Q}(k)\boldsymbol{q}_0 = \boldsymbol{0} \tag{3}$$

where $\boldsymbol{q}_0$ is assumed to be free of flutter and $\Delta q_D \equiv q_D - q_{D_0}$. Computing the transfer function from $\boldsymbol{q}_0$ to $\boldsymbol{\Delta q}$, we get

$$\begin{aligned} \boldsymbol{G}(\omega) &\equiv [-\omega^2\boldsymbol{M} + j\omega\boldsymbol{C} + \boldsymbol{K} - q_D\boldsymbol{Q}(k)]^{-1}\Delta q_D\boldsymbol{Q}(k) \\ &= [-\omega^2\boldsymbol{M} + j\omega\boldsymbol{C} + \boldsymbol{K} - q_D\boldsymbol{Q}(k)]^{-1}[-\omega^2\boldsymbol{M} + j\omega\boldsymbol{C} + \boldsymbol{K} - q_{D_0}\boldsymbol{Q}(k)] - \boldsymbol{I}_N \\ &\equiv \boldsymbol{T}(\omega)\boldsymbol{T}_0^{-1}(\omega) - \boldsymbol{I}_N \end{aligned} \tag{4}$$

where the frequency responses, $\boldsymbol{T}_0(\omega)$ and $\boldsymbol{T}(\omega)$ are obtained at the two subcritical dynamic pressures, q_{D_0}, q_D, respectively. Taking eigen decomposition of (4) yields,

$$\boldsymbol{G}(\omega) \equiv \boldsymbol{V}_N(\omega)\boldsymbol{\Lambda}_N(\omega)\boldsymbol{W}_N^T(\omega) \tag{5}$$

where

$$\boldsymbol{\Lambda}_N(\omega) = (N \times N) \text{ diagonal matrix with dynamic eigenvalues}$$
$$\boldsymbol{V}_N(\omega),\ \boldsymbol{W}_N(\omega) = (N \times N) \text{ matrices of right and left dynamic eigenmodes}$$
$$\boldsymbol{V}_N(\omega)\boldsymbol{W}_N^{\dagger}(\omega) = \boldsymbol{I}_N \quad \textit{(orthonormality)}$$

It can be shown that the dynamic eigenmodes of the aeroelastic system are *invariant to dynamic pressure* [14]. That is, if we repeat the eigen decomposition at another dynamic pressure, say at q_{D_0}, we will get.

$$\boldsymbol{G}_0(\omega) \equiv \boldsymbol{V}_N(\omega)\boldsymbol{\Lambda}'_N(\omega)\boldsymbol{W}_N^T(\omega) \tag{6}$$

and the dynamic eigenvalues at q_D and q_{D0} are related by

$$\boldsymbol{\Lambda}_N(\omega) = [\boldsymbol{I}_N - \boldsymbol{\Lambda}'_N(\omega)]^{-1}\boldsymbol{\Lambda}'_N(\omega) \tag{7}$$

Suppose that the dynamic pressure is increased from q_D to $q_D + k\Delta q_D$. Then, the new eigenvalues at $q_D + k\Delta q_D$ are,

$$[\boldsymbol{I}_N - k\boldsymbol{\Lambda}_N(\omega)]^{-1}k\boldsymbol{\Lambda}_N(\omega) \tag{8}$$

while the dynamic eigenmodes remain unchanged. Therefore, the aeroelastic instability, i.e., flutter, is found by the condition:

$$1 - k_f\lambda_{Ni}(\omega_f) = 0 \tag{9}$$

for at least one of the indices, $i = 1,2,\dots,N$. See Fig. 1. The critical flutter dynamic pressure is $q_{Df} = q_D + k_f\Delta q_D$. Equally important, it can be shown that *the flutter mode is indeed one of the invariant dynamic eigenvectors, $\boldsymbol{v}_{Ni}(\omega_f)$, at the critical frequency, ω_f* [14]. This conclusion implies that a flutter mode is an intrinsic property of the aeroelastic system independent of the dynamic pressure, rather than the solution pertaining to the flutter condition.

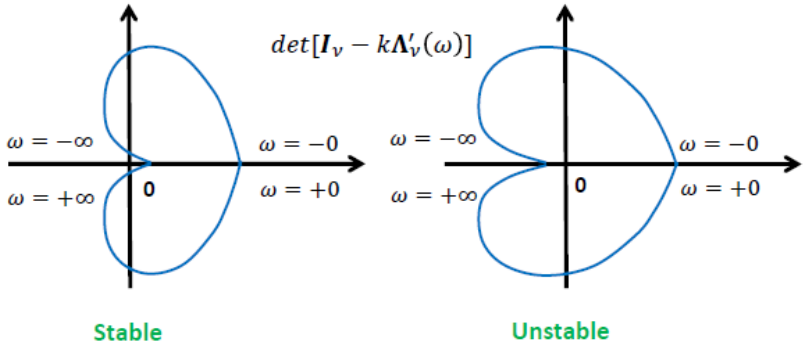

Fig. 1 Stable and unstable systems according to Nyquist Stability [20]

It is mentioned that in reality getting the $(N \times N)$ modal responses $\boldsymbol{G}(\omega)$ is difficult because we do not have a sufficient number of actuators to excite the modes. On the other hand, one can always install as many sensors as necessary. Kim [15] resolves this issue by replacing the $(N \times N)$ data

with data due to limited inputs obtained at multiple flight points. We will assume that as a prerequisite for LCO prediction this approach has been implemented and used to conduct the FFT.

3 EXTENSION TO LIMIT CYCLE OSCILLATION

In essence, all of the above logic and schemes developed for the prediction of the linear dynamic instability are applicable to LCOs. However, the dynamic instability determined by (9) should be interpreted differently in the following sense. An LCO with a specified amplitude level exists at the critical point with a zero effective aeroelastic damping allowing the oscillation to sustain in a steady-state fashion. Under the quasi-linear assumption, it implies that the sustained oscillation has only one major harmonic component. Thus, this type of solution is equivalent to that of a harmonic balance method for general nonlinear analysis where only harmonic terms of a major frequency, $\sin(\omega t), \cos(\omega t)$ are retained with all other higher harmonics neglected.

3.1 Fourier Analysis of Nonlinear Freeplay and Equivalent Stiffness

Considering that we deal with only structural nonlinearity, it is natural and reasonable to approximate the nonlinear motion about the control surface hinge axis using the Fourier Analysis. See Fig. 2 for the bilinear nature of the stiffness curve where a gap of δ is allowed in the control surface freeplay angle. Expressing the hinge moment in a sinusoidal motion and the equivalent stiffness $K_{\beta eq}$, the Fourier Transformation leads to [19]:

$$M_\beta(t) = B_1 sin\omega t = \frac{B_1}{\beta_R}\beta_R sin\omega t = K_{\beta eq}\beta \tag{10}$$

$$K_{\beta eq} = \frac{B_1}{\beta_R} = \frac{K_\beta}{\pi}\left(\pi - 2arcsin\frac{\delta}{\beta_R} - 2\frac{\delta}{\beta_R}\sqrt{1-(\frac{\delta}{\beta_R})^2}\right) \ (K_\beta = \text{the nominal stiffness}) \tag{11}$$

.

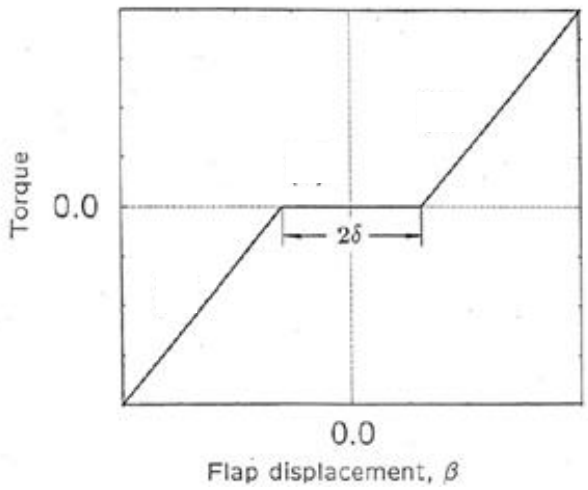

Fig. 2 Bilinear stiffness of a symmetric freeplay [19]

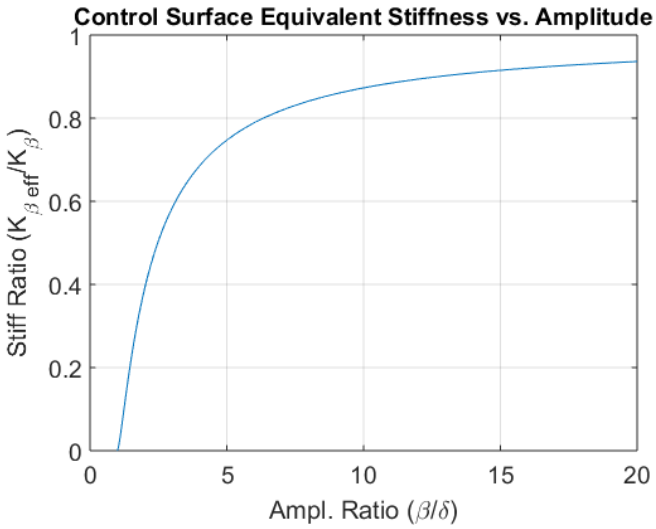

Fig. 3 Equivalent stiffness curve vs. non-dimensional rotation angle

Fig. 3 shows the graph of the equivalent stiffness ratio as a function of the amplitude ratio, β/δ.

3.2 Dynamic Eigen Decomposition with Two Parameter Variations

The prediction of LCO using DED proceeds as follows. First, let $\Delta\boldsymbol{K}$ represent an increment in the stiffness matrix from the nominal stiffness $\boldsymbol{K}_0$ due to the change in the control surface stiffness. As in the case with the variation in dynamic pressure q_D, we need a transfer function whose DED will yield dynamic eigenvalues and eigenmodes necessary to check the new dynamic instability:

$$\boldsymbol{G}_K(\omega) \equiv [-\omega^2\boldsymbol{M} + j\omega\boldsymbol{C} + \boldsymbol{K}_0 - q_D\boldsymbol{Q}(k)]^{-1}(-\boldsymbol{\Delta K}) \tag{12}$$

where assuming the control surface with freeplay is in the last degree-of-freedom,

$$\boldsymbol{\Delta K} \equiv \begin{bmatrix} 0 & \cdots & 0 \\ \vdots & \ddots & \vdots \\ 0 & \cdots & \delta K_{\beta eq} \end{bmatrix} \tag{13}$$

For LCO calculations, the nominal stiffness for the hinge axis is set to be zero. That is, $K_{\beta 0} = 0$. Since $rank(\Delta\boldsymbol{K}) = 1$ we expect the DED of (12) will have a single nonzero dynamic eigenvalue. Hence, we can use the following (1×1) transfer function instead:

$$g_K(\omega) \equiv -\boldsymbol{c}_K[-\omega^2\boldsymbol{M} + j\omega\boldsymbol{C} + \boldsymbol{K}_0 - q_D\boldsymbol{Q}(k)]^{-1}\boldsymbol{\Delta k} \tag{14}$$

where $\boldsymbol{c}_K$ is the sensor matrix for the control surface rotational angle:

$$\boldsymbol{c}_K \equiv \lfloor 0 \quad \cdots \quad 0 \quad 1 \rfloor \quad (1 \times N) \tag{15}$$

and $\boldsymbol{\Delta k}$ is the last column of $\boldsymbol{\Delta K}$. Note that $g_K(\omega)$ should be available from the FFT provided that the flutter testing has already taken place, although in the present formulation the dynamics of the actuator connected to the control surface is ignored for simplicity of the expression [21].

Next, get dynamic eigen decomposition of the rank 1 function (14):

$$g_K(\omega) \equiv v_K(\omega)\lambda'_K(\omega)w_K^T(\omega) \tag{16}$$

Suppose the control surface stiffness changes by $m\boldsymbol{\Delta k}$ from the nominal value, or the amplitude of the control surface changes following the $K_{\beta eq}$ vs. $\frac{\beta}{\delta}$ curve (Fig. 3). Then, according to the Nyquist Stability the stability of the new system with $\boldsymbol{K}_0 + m\boldsymbol{\Delta K}$ at q_D can be determined by checking the new dynamic eigenvalue, $\lambda_k \equiv m\lambda'_K/(1 - m\lambda'_K)$. That is, an LCO point and its solution are found by the condition, $|1 - m_c\lambda'_K(\omega_c)| = 0$.

One can vary the stiffness with Eq. (16), but it is valid only at the fixed dynamic pressure. In reality, the critical dynamic pressure for an LCO is not known a priori, nor the transfer function can be obtained at the critical speed. Therefore, it is preferable to consider a transfer function,

$$g_{KD}(\omega) \equiv -\boldsymbol{c}_K\left[-\omega^2\boldsymbol{M} + j\omega\boldsymbol{C} + \boldsymbol{K}_0 - (q_{D_0} + l\Delta q_D)\boldsymbol{Q}(k)\right]^{-1}\boldsymbol{\Delta k} \tag{17}$$

where q_{D_0} is a reference dynamic pressure used during the FFT so that the dynamic instability or LCO can be sought by varying both q_D and $\boldsymbol{K}$, i.e., l and m. Towards this end, note

$$\begin{aligned}&\left[-\omega^2\boldsymbol{M} + j\omega\boldsymbol{C} + \boldsymbol{K}_0 - (q_{D_0} + l\Delta q_D)\boldsymbol{Q}(k)\right]^{-1}\boldsymbol{\Delta k} = \\ =&< \boldsymbol{I} - l\left[-\omega^2\boldsymbol{M} + j\omega\boldsymbol{C} + \boldsymbol{K}_0 - q_{D_0}\boldsymbol{Q}(k)\right]^{-1}\Delta q_D\boldsymbol{Q}(k) >^{-1} \\ &\cdot\left[-\omega^2\boldsymbol{M} + j\omega\boldsymbol{C} + \boldsymbol{K}_0 - q_{D_0}\boldsymbol{Q}(k)\right]^{-1}\boldsymbol{\Delta k}\end{aligned} \tag{18}$$

In the above expression, from (4)-(6) we have $[-\omega^2\boldsymbol{M} + j\omega\boldsymbol{C} + \boldsymbol{K}_0 - q_{D_0}\boldsymbol{Q}(k)]^{-1}\Delta q_D\boldsymbol{Q}(k) = \boldsymbol{V}_N(\omega)\boldsymbol{\Lambda}'_N(\omega)\boldsymbol{W}_N^T(\omega)$**.** On the other hand, $\left[-\omega^2\boldsymbol{M} + j\omega\boldsymbol{C} + \boldsymbol{K}_0 - q_{D_0}\boldsymbol{Q}(k)\right]^{-1}\boldsymbol{\Delta k}$ is the response of the modal degrees-of-freedom due to the control surface excitation. As explained earlier, we cannot have the full $(N \times N)$ transfer function matrix due to lack of inputs (for instance, we have six at most for a conventional airplane with flaps, ailerons, an elevator, and a rudder). Following Ref. [15] in which the $(N \times N)$ modal response is replaced with $(M \times M)(M < N)$ sensor outputs obtained at multiple flight points, we will approximate

$$\begin{aligned}g_{KD}(\omega) &\approx \boldsymbol{c}_K\boldsymbol{V}_v(\omega)[\boldsymbol{I} - l\boldsymbol{\Lambda}'_v(\omega)]^{-1}\boldsymbol{W}_v^T(\omega)\boldsymbol{g}_{KC}(\omega) \\ &\equiv v_K(l,\omega)\lambda'_K(l,\omega)w_K^T(l,\omega)\end{aligned} \tag{19}$$

$$\begin{aligned}\boldsymbol{c}_K &\equiv \lfloor 0 \quad \cdots \quad 1 \rfloor \ (1 \times M) \\ \boldsymbol{V}_v, \boldsymbol{\Lambda}'_\boldsymbol{v}, \boldsymbol{W}_v &\equiv DED\ of\ (M \times M)\ responses\ due\ to\ limited \\ &\quad number\ of\ inputs\ at\ multiple\ flight\ conditions \\ \boldsymbol{g}_{KC}(\omega) &\equiv (M \times 1)\ sensor\ responses\ due\ to\ the\ control\ surface\ excitation\end{aligned}$$

$$= -\boldsymbol{C}\left[-\omega^2\boldsymbol{M} + j\omega\boldsymbol{C} + \boldsymbol{K}_0 - q_{D_0}\boldsymbol{Q}(k)\right]^{-1}\boldsymbol{\Delta k} \tag{20}$$

It is emphasized again that all of $\boldsymbol{V}_\nu, \boldsymbol{\Lambda}'_\nu, \boldsymbol{W}_\nu$ and $\boldsymbol{g}_{KC}$ are available already from the previous FFT. The premise of using (19) in lieu of (17) is that in so far as the eigen structure of the full matrix is well captured by the smaller matrix it will yield accurate information about LCO as it does for linear flutter. Using (19) it is now possible to vary both q_D and $\boldsymbol{\Delta k}$ independently by the two scalars, l and m to find an LCO that satisfies

$$1 - m_c\lambda'_K(l_c,\ \omega_c) = 0 \tag{21}$$

This procedure is similar to that of linear flutter prediction except that we now have two, instead of one, parameters to vary (Fig. 4).

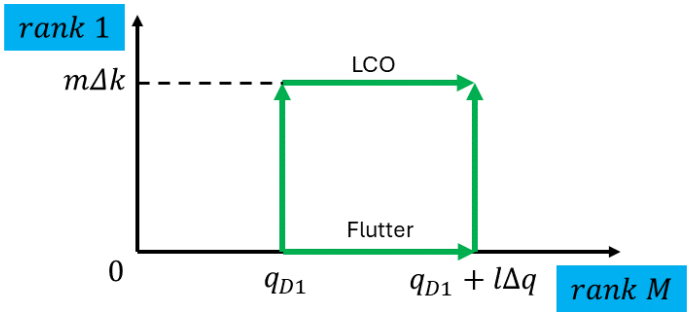

Fig. 4 Parameter variations along two paths for LCO prediction.

3.3 Identification of LCO Mode

One question remains: how do we identify an LCO mode? Is it possible to find the mode from the pre-existing data as it was for a flutter mode? In the case of flutter, it was proven that one of the dynamic eigenmodes at the critical frequency is identical to the flutter mode and it is independent of dynamic pressure [14]. Can we draw a similar conclusion for the case of LCO prediction? To answer these questions, let's examine the following $(N \times N)$ modal transfer function:

$$\begin{aligned}&\left[-\omega_c^2\boldsymbol{M} + j\omega_c\boldsymbol{C} + \boldsymbol{K}_0 - (q_{D_0} + l_c\Delta q_D)\boldsymbol{Q}(k_c)\right]^{-1}(-\boldsymbol{\Delta K})\\ &\quad\equiv \boldsymbol{v}_{Kt}(l_{c,}\ \omega_c)\lambda'_{Kt}(l_c, \omega_c)\boldsymbol{w}_{Kt}^T(l_c, \omega_c)\end{aligned} \tag{22}$$

Note that since $rank(\boldsymbol{\Delta K}) = 1$, Eq. (22) yields only one non-zero dynamic eigenvalue λ'_{Kt}. Therefore, with only one non-zero column available in the transfer function matrix the $(N \times 1)$ forced response due to the control surface excitation, $\left[-\omega_c^2\boldsymbol{M} + j\omega_c\boldsymbol{C} + \boldsymbol{K}_0 - (q_{D_0} + l_c\Delta q_D)\boldsymbol{Q}(k_c)\right]^{-1}\boldsymbol{\Delta k}$ becomes the dynamic eigenvector $\boldsymbol{v}_{Kt}(l_c, \omega_c)$ corresponding to the non-zero dynamic eigenvalue.

If the aeroelastic system has an LCO solution at the critical condition, (l_c, m_c, ω_c), then

$$\left[-\omega_c^2\boldsymbol{M}+j\omega_c\boldsymbol{C}+(\boldsymbol{K}_0+m_c\boldsymbol{\Delta K})-(q_{D_0}+l_c\Delta q_D)\boldsymbol{Q}(k_c)\right]^{-1}(-m_c\boldsymbol{\Delta K})$$
$$=\boldsymbol{v}_{Kt}(l_c,\omega_c)\lambda_{Kt}(l_c,m_c,\omega_c)\boldsymbol{w}_{Kt}^T(l_c,\omega) \quad (23)$$

will diverge because $\lambda_{Kt}(l_c,m_c,\omega_c)\equiv m_c\lambda'_{Kt}/(1-m_c\lambda'_{Kt})$ diverges. Pre-multiplying both sides of (23) by $-\omega_c^2\boldsymbol{M}+j\omega_c\boldsymbol{C}+(\boldsymbol{K}_0+m_c\boldsymbol{\Delta K})-(q_{D_0}+l_c\Delta q_D)\boldsymbol{Q}(k_c)$ yields,

$$-m_c\boldsymbol{\Delta K}=[-\omega_c^2\boldsymbol{M}+j\omega_c\boldsymbol{C}+(\boldsymbol{K}_0+m_c\boldsymbol{\Delta K})$$
$$-(q_{D_0}+l_c\Delta q_D)\boldsymbol{Q}(k_c)]\boldsymbol{v}_{Kt}(l_c,\omega_c)\lambda_{Kt}(l_c,m_c,\ \omega_c)\boldsymbol{w}_K^T(l_c,\omega) \quad (24)$$

Since $\boldsymbol{\Delta K}$ is *finite* but $\lambda_{Kt}(l_c,m_c,\ \omega_c)\ \to\infty$ we require,

$$[-\omega_c^2\boldsymbol{M}+j\omega_c\boldsymbol{C}+(\boldsymbol{K}_0+m_c\boldsymbol{\Delta K})-(q_{D_0}+l_c\Delta q_D)\boldsymbol{Q}(k_c)]\boldsymbol{v}_{Kt}(l_c,\omega_c)=\boldsymbol{0} \quad (25)$$

That is, $\boldsymbol{v}_{Kt}(l_c,\omega_c)$ *or the forced modal response due to the single control surface excitation at the critical condition is the LCO mode.* Remember that we can only estimate the mode approximately because we have only the sensor measurements available. With this limitation aside, we can expect that the single dynamic eigenvector of the corresponding $(M\times M)$ transfer function or *the* $(M\times 1)$ *forced response due to the single control surface input* will closely approximate $\boldsymbol{v}_{Kt}(l_c,\omega_c)$ of the full transfer function (22) and hence will be the LCO mode. It goes without saying that the LCO mode can be extracted entirely based on the pre-existing FFT data.

4 NUMERICAL SIMULATION OF FLIGHT: TAPERED WING WITH FLAPS IN SUBSONIC INCOMPRESSIBLE FLOW

For demonstration of the newly proposed LCO prediction methodology, a tapered but unswept wing with four flaps is studied. The clean wing is a model originally created for aeroelasticity classes taught at MIT, National University of Singapore, and University of Washington. For the purpose of modeling the control surfaces and excitation of the wing, four flaps are attached along the trailing edge of this wing. The wing's span is 40 ft, its chord is 22.6 ft, 14.6 ft at the root and tip, respectively. Each flap is 3.5 ft in chord, 10 ft in span. Details of the modeling can be found in Ref. [15].

4.1 Structural and Aerodynamic Modeling

Fig. 5 is a top view of the wing and flaps. For structural modeling, a total of ten uncoupled modes are used for the wing [22], while the flaps are modeled by a rigid rotational mode neglecting elasticity. A structural damping of 3% is assumed in all of the modes. Four pairs of sensors are located along the elastic axis. Each pair measures the vertical deflections and rotational angles at the locations. Additionally, four sensors are located along the hinge axis to measure the rotational angles of the flaps. Thus, we have a total of twelve measurements and four excitations. See Fig. 6.

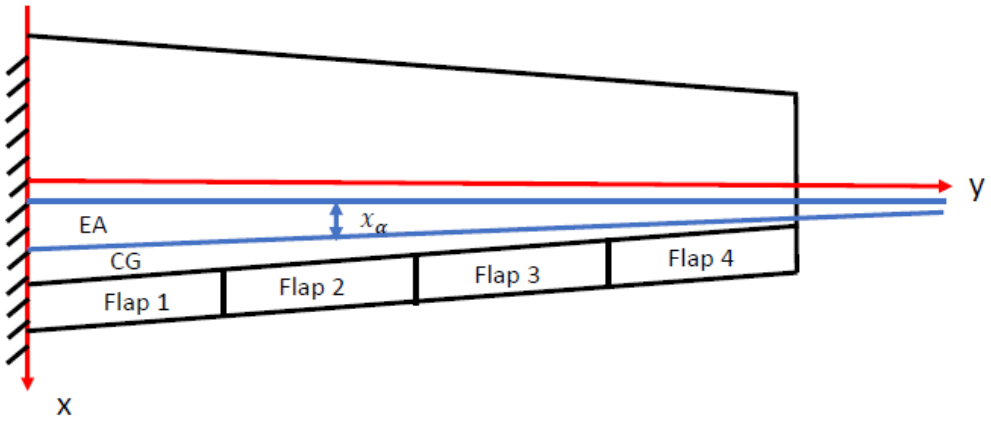

Fig. 5 Schematic diagram of tapered wing with four flaps.

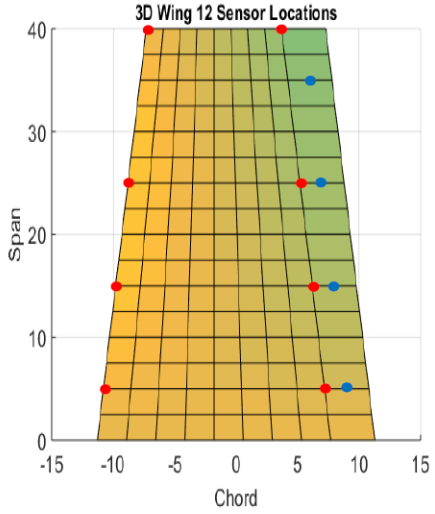

Red=translational
Blue=rotational
All four (#1,2,3,4) flaps are used along the trailing edge.

Fig. 6 Sensor locations for soft hinged wings/flaps.

For aerodynamic modeling, the incompressible and inviscid unsteady aerodynamic theory by Theodorsen is used accounting for the motion of the trailing edge control surface [23]. To express the unsteady aerodynamics in time-domain, one pole Pade approximation of the circulatory term is adopted. Aeroelastic modeling of the wing-flaps is done by coupling the structural dynamic equation with the unsteady aerodynamic equation. The size of the aeroelastic system matrix is (42×42). Following the CMVA practice, air speed was fixed at $V_\infty = 511.9\, ft/sec$ and the dynamic pressure was varied by changing air density alone. In a flight situation, this would be equivalent to descending in altitude following a constant Mach curve fixed approximately at $M_\infty = .5$.

4.2 Flight Flutter Testing Simulation

It is assumed that during the FFT there were no freeplays existing in the control surface hinges and all the data collected are about the clean wing with flaps without structural nonlinearity. This is a reasonable assumption because a test aircraft that was newly manufactured should not have such structural defects yet. Likewise, no control surface freeplays were included in numerical simulations of the FFT.

From the exact eigenvalue analysis of the state-space aeroelastic equation of motion, the wing with the soft hinges and with nominal flap stiffness (i.e., no freeplay) is known to flutter at $q_{Df0} = 453.8\ \frac{slug}{ft\ sec^2}, \omega_{f0} = 5.1\ Hz$. Fig. 7 is a Nyquist plot reproduced from Ref. [15] at the nominal flutter condition resulting from the DED processing using the (14×14) modal responses and (12×4) sensor measurements, respectively. The dynamic instability is indicated by the touching of the origin. Both predictions agree extremely well with the result from eigenvalue analysis.

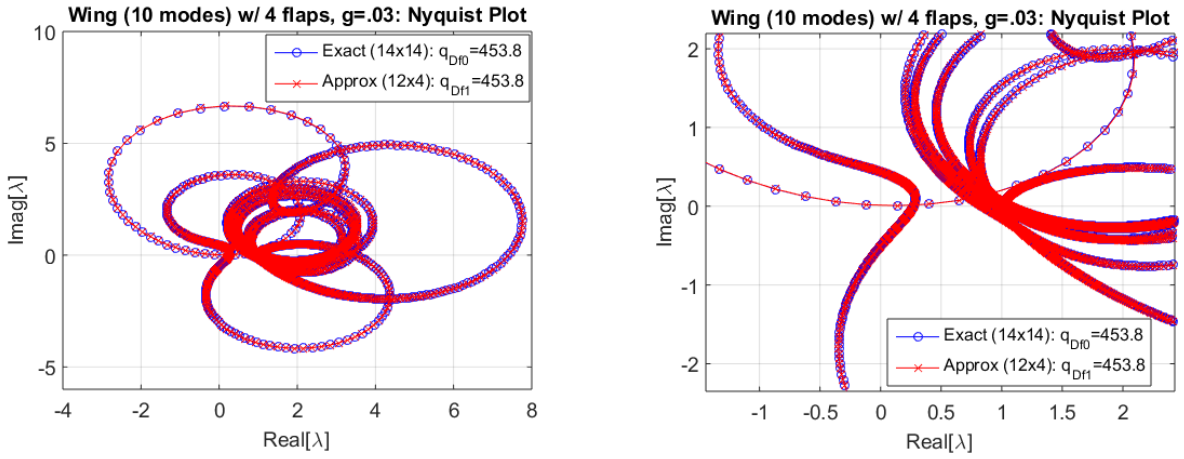

Fig. 7 Nyquist plot with nominal stiffness at $q_{Df} = 453.8\frac{slug}{ft\ sec^2}$ (4 actuators, 12 sensors).

4.3 Prediction of Limit Cycle Oscillations

To investigate LCOs due to the control surface nonlinearity, we introduce a freeplay in flap #4 (the most outboard, closest to the wing tip). Without specifying the gap angle δ, Eq. (21) allows to predict LCO in terms of the scalar multiple m given an incremental stiffness $\boldsymbol{\Delta K}$ from the nominal stiffness $\boldsymbol{K}_0$. To test out the new scheme, we initially set $m = 0, \boldsymbol{\Delta K} = \boldsymbol{K}_0$ retaining 0% of the nominal hinge stiffness and varied the dynamic pressure. Based on the data processing using the DED formulation (19)-(21), we found that for the 100% reduction in the stiffness the LCO solution requires 63.1% decrease in the dynamic pressure, $q_{D_c} = 167.3\frac{slug}{ft\ sec^2}$. From Fig. 3 this corresponds to an amplitude ratio $0 \leq \frac{\beta}{\delta} \leq 1$. The LCO frequency is found to be 1.05 Hz. This Nyquist plot is shown in Fig. 8. Clearly, although it could not be found in the flutter prediction it is also a linear flutter solution with zero hinge stiffness in flap #4. Similarly, a second LCO point

with $0 \leq \frac{\beta}{\delta} \leq 1$ was also found at a higher dynamic pressure, $q_{Dc} = 389.1 \frac{slug}{ft\ sec^2}$ with $\omega_f = 4.99\ Hz$, but we will focus on LCOs emanating from the first solution at $q_{Dc} = 167.3 \frac{slug}{ft\ sec^2}$.

It is reported that for LCO predictions both the (14×14) modal responses and (12×4) sensor responses were used but no noticeable differences were found in the results. For this reason, only results from the (12×4) sensor responses are presented in all of figures that follow in this section.

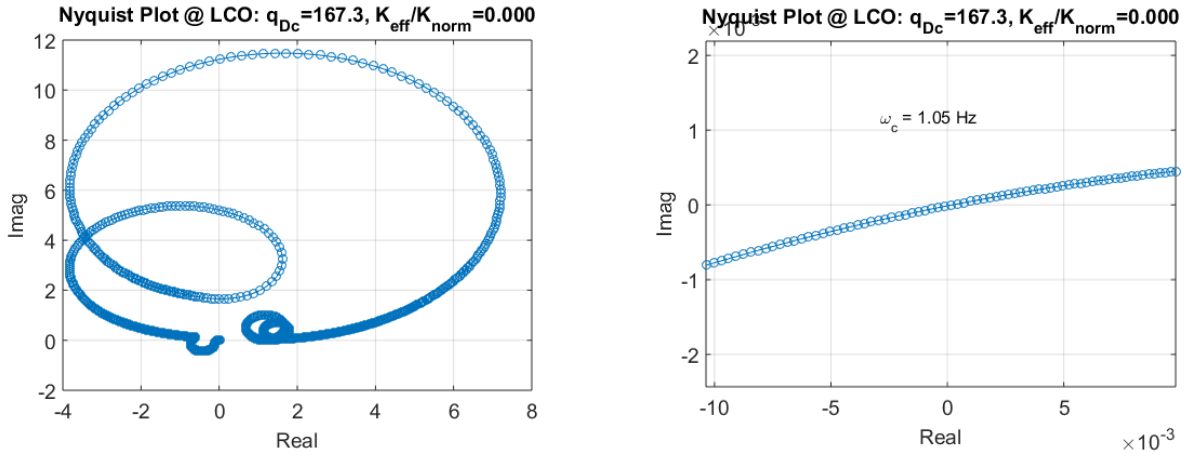

Fig. 8 Nyquist plot of LCO with zero stiffness in the 4th flap at $q_{Dc} = 167.3 \frac{slug}{ft\ sec^2}$.

Next, we set $m = -.975$ retaining only 2.5% of the nominal hinge stiffness and varied the dynamic pressure around the linear flutter point at $167.3 \frac{slug}{ft\ sec^2}$ For the 97.5% reduction in the stiffness the LCO solution requires 18.1% decrease in the dynamic pressure, i.e., $q_{D_c} = 137 \frac{slug}{ft\ sec^2}$. From Fig 3. this solution corresponds to an amplitude ratio of $\frac{\beta}{\delta} = 1.08$. The LCO frequency is 1.29 Hz. Fig. 9 shows the Nyquist plot.

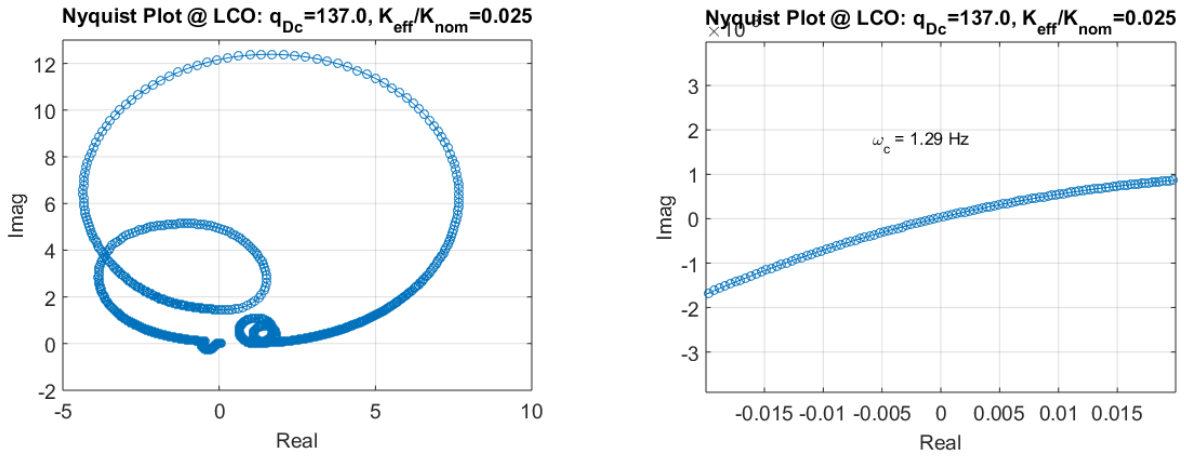

Fig. 9 Nyquist plot of LCO with 2.5% nominal stiffness in the 4th flap at $q_{Dc} = 137 \frac{slug}{ft\ sec^2}$.

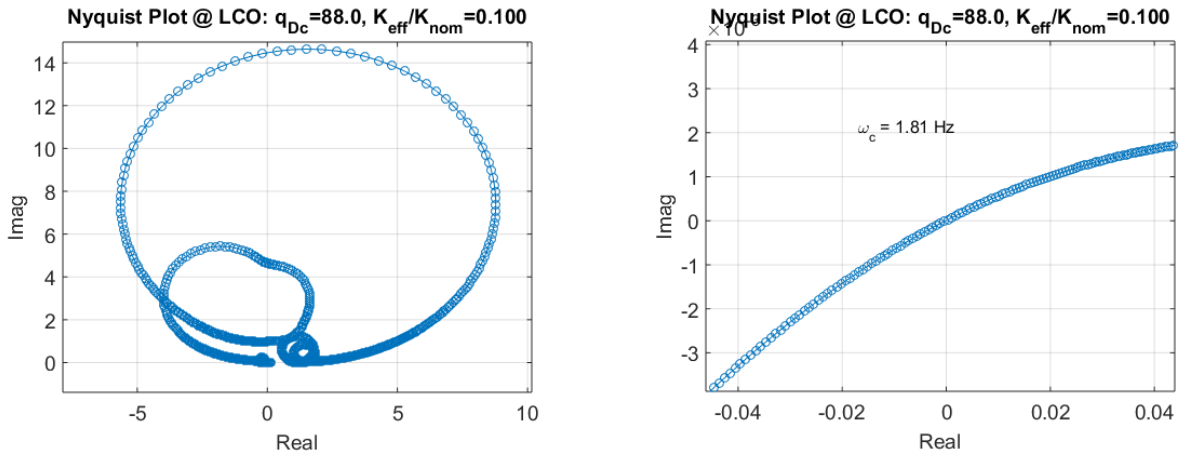

Fig. 10 Nyquist plot of LCO with 10% nominal stiffness in the 4th flap at $q_{Dc} = 88 \frac{slug}{ft\ sec^2}$.

Fig. 10 is another LCO result at $88 \frac{slug}{ft\ sec^2}$ where the effective hinge stiffness has increased to 10% of the nominal stiffness while the flap amplitude ratio has increased to 1.24δ and the LCO frequency is 1.81 Hz. Comparing the two consecutive solutions, Figs. 9 and 10, we can expect a 'softening' LCO branch forming here because an increase in the flap amplitude resulted in a decrease in critical dynamic pressure.

Fig. 11 and 12 are LCO results at 81 and $160 \frac{slug}{ft\ sec^2}$, respectively, but unlike the previous two cases the amplitude increases as dynamic pressure is increased. It appears that an another LCO branch is forming at an upper level of amplitudes with the β vs. q_D trend reversed.

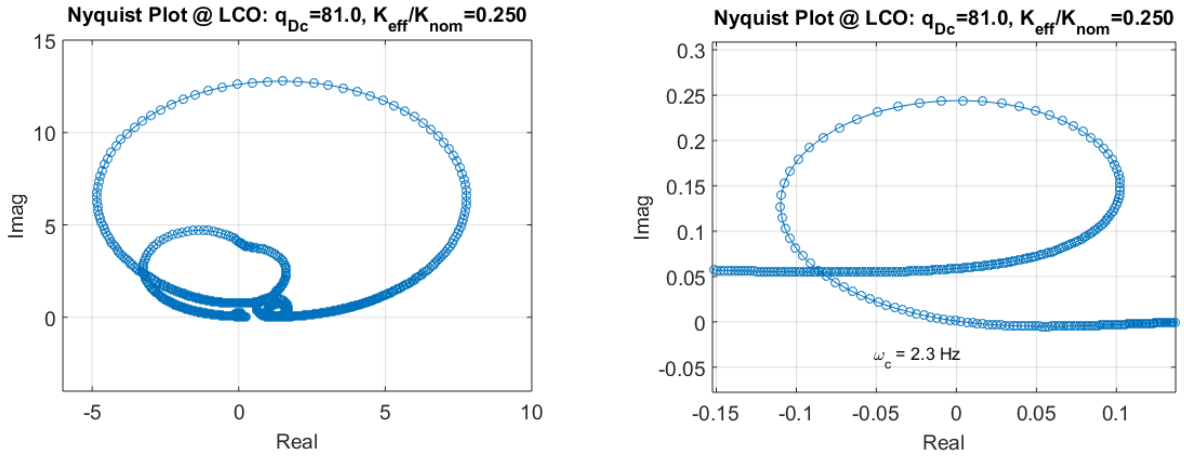

Fig. 11 Nyquist plot of LCO with 25% nominal stiffness in the 4th flap at $q_{Df} = 81 \frac{slug}{ft\ sec^2}$.

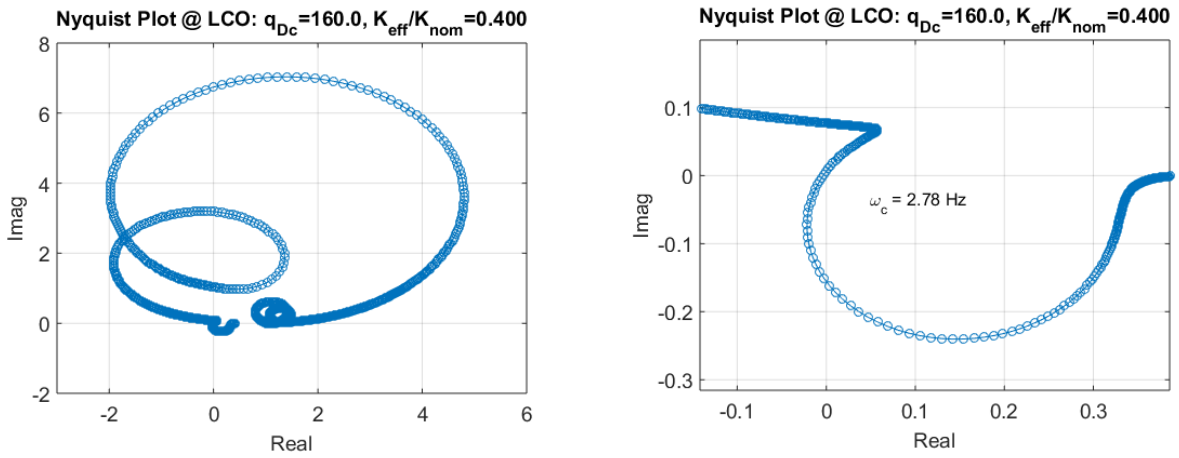

Fig. 12 Nyquist plot of LCO with 40% nominal stiffness in the 4th flap at $q_{Df} = 160 \frac{slug}{ft\ sec^2}$.

Collecting all the LCO solutions predicted and investigated together, we have Fig. 13 in which the amplitude ratios of the flap #4 are plotted against critical dynamic pressures. As expected, there are two LCO branches forming a 'softening' or 'bad' group of LCOs. The lower branch which starts at $q_{Dc} = 167.3 \frac{slug}{ft\ sec^2}$ merges with the upper branch at $q_{Dc} = 73 \frac{slug}{ft\ sec^2}$ and then continues to increase the amplitude following the branch. The frequency at which these LCOs oscillate gradually increases along the branch ranging from 1.05 Hz for $\frac{\beta}{\delta} = 1$ to 3.46 Hz for with $\frac{\beta}{\delta} = 4.25$.

Checking LCO modes based on (23) reveals that they consist of mostly a low frequency wing bending mode coupled with angular deflections in flap #4. In other words, they are characterized mostly by the local control surface motion in the flap undergoing the freeplay. See Fig. 14 for the real and imaginary parts of the identified LCO mode at 88 $\frac{slug}{ft\ sec^2}$ (NOTE: the LCO modes displayed in Figs 14, 15 are not scaled as per their specified amplitude ratios.). As the amplitude increases further matters get complicated because we will run into another group of LCOs in the higher region of dynamic pressure starting at around $355.1 \frac{slug}{ft\ sec^2}$. As can be seen from Fig. 13, although they display the same characteristics of the 'softening' LCOs the amplitudes involved are much bigger. Checking LCO modes on this branch confirms that they stem from the linear flutter mode that starts at $389.1 \frac{slug}{ft\ sec^2}$ with zero stiffness in flap #4. See Fig. 15 for the identified LCO mode at $368.7 \frac{slug}{ft\ sec^2}$ and compare it with the identified linear flutter mode from Ref. [15]. It can be seen that this mode contains motions in all four flaps as well as wing torsion. These LCO modes are indeed the same as frequency responses due to the control surface excitations in flap #4 at 1.24 Hz and 2.24 Hz, respectively, confirming what was found earlier in Section 3.3.

Without performing nonlinear stability analysis, it is reasonable to suspect that the lower branches shown in Fig 13 would indicate unstable LCOs whereas the upper ones represent stable LCOs. Unstable in that if the flap #4 is kicked by a small disturbance the oscillation will die out but if it is kicked by a moderate to large amount of disturbance it will lead to an explosive vibration with

a very large amplitude. Worse still, it will pass through the lower branch and jump right up to the upper branch with a larger, catastrophic motion. More importantly, these LCOs can occur at speeds much lower than the nominal flutter speed. All of these properties of the softening LCOs could potentially lead to serious fatigue and safety issues making it imperative to avoid them during the design and analysis phases of aircraft.

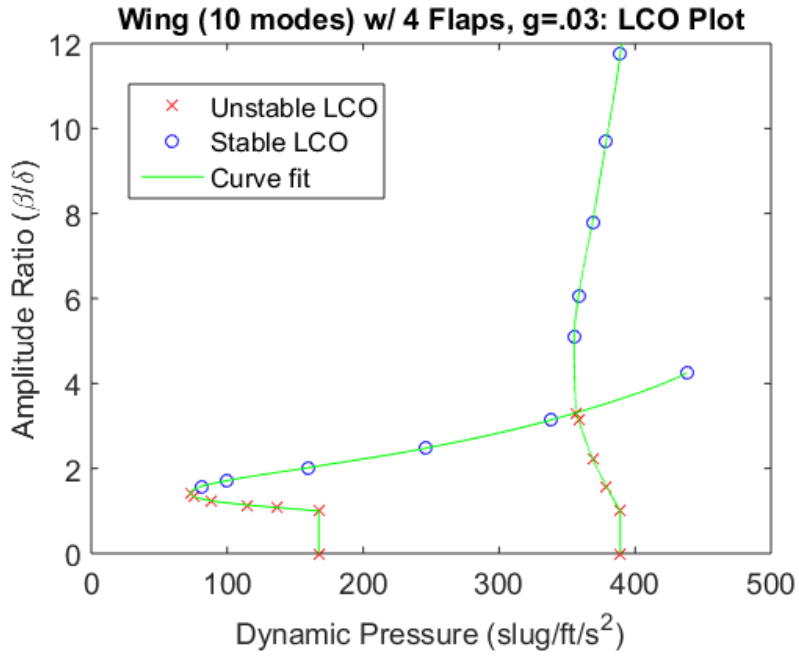

Fig. 13 LCO branch: amplitude ratio vs. critical dynamic pressure.

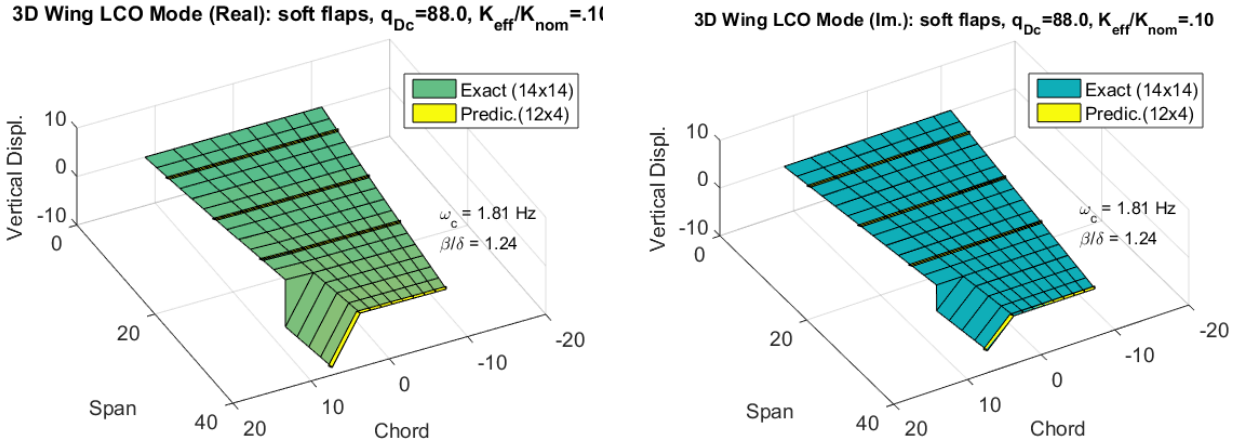

Fig. 14 LCO mode of the soft hinged wing at $q_{Dc} = 88\frac{slug}{ft\ sec^2}, \frac{\beta}{\delta} = 1.24$ (4 actuators, 12 sensors).

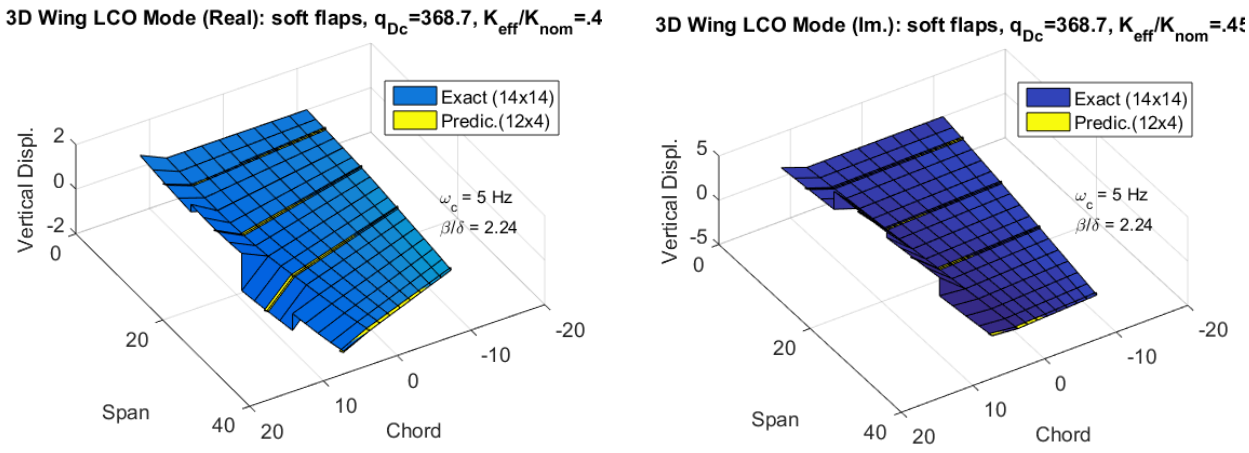

Fig. 15 LCO mode of the soft hinged wing at $q_{Dc} = 368.7 \frac{slug}{ft\ sec^2}, \frac{\beta}{\delta} = 2.24$ (4 actuators, 12 sensors).

5 CONCLUDING REMARKS

In this work, a new LCO prediction methodology based on flight test data has been developed using the Dynamic Eigen Decomposition (DED) and the Nyquist stability theorem. Previously, the DED was used for predicting flutter boundaries [14, 15], but here it is modified to account for large amplitude nonlinear effects emanating from the nonlinearities existing within the system. For this work, the main focus is on structural nonlinearity due to a single-degree control surface freeplay. By using Fourier transform technique and the DED, it was shown that the essential characteristics of the nonlinear aeroelastic phenomenon are well captured as long as the first harmonics are a major content in the nonlinearity responses. Interestingly, it was proven that an LCO mode at a critical condition is identical to its dynamic eigenmode or equivalently, a forced response due to the control surface excitation. Whereas the linear flutter prediction requires varying only one parameter, the LCO prediction requires variations in two-dimensional parameter space, i.e., dynamic pressure and amplitude level. More importantly, for the proposed scheme to work no additional data beyond the flight flutter test (FFT) data is required and LCOs can be predicted entirely by manipulating the pre-existing data alone. This should be a great advantage when conducting FFT for the purpose of flutter prediction and LCO prediction as well.

It was shown in the numerical simulations of a tapered wing with four flaps that the proposed approach can predict LCOs with high accuracy and robustness. In this study, aerodynamic nonlinearities due to large motions such as dynamic stall, shocks were not considered, and aerodynamics was assumed to be statistically nonlinear but dynamically linearized. Hence, using the method must be restricted to subsonic and supersonic flights with moderate ranges of amplitudes. More research needs to be done including the aerodynamic nonlinearities and multiple control surface freeplays. Needless to say, the method must be validated using real flight test data.

Acknowledgement

This material is based upon work partially supported by the National Aeronautics and Space Administration under Grant No. 80NSSC23M0060 issued through the University Leadership Initiative Program. Any opinions, findings and conclusions or recommendations expressed in this material are those of the author and do not necessarily reflect the views of NASA.

REFERENCES

[1] Lind, R., Brenner, M., 2000. Flutterometer: An On-Line Tool to Predict Robust Flutter Margins. Journal of Aircraft. 37 (6), 1105-1112.

[2] Dimitriadis, G., Cooper, J.E., 2001. Flutter Prediction from Flight Flutter Test Data. Journal of Aircraft. 38 (2), 355-367.

[3] Kehoe, M.W., 1995. A Historical Overview of Flight Flutter Testing. NASA TM-4720.

[4] Cooper, J.E., Emmett, P.R., Wright, J.R., 1993. Envelope Function-A Tool for Analyzing Flutter Data. Journal of Aircraft. 30 (5), 785-790.

[5] Zimmerman, N.H., Weissenburger, J.T., 1964. Prediction of Flutter Onset Speed Based on Flight Testing at Subcritical Speeds. Journal of Aircraft. 1 (4), 190-202.

[6] Torii, H., Matsuzaki, Y., 2001. Flutter Margin Evaluation for Discrete-Time Systems. Journal of Aircraft. 38 (1), 42-47.

[7] Lind, R., Brenner, M., 2000. Flutterometer: An On-Line Tool to Predict Robust Flutter Margins. Journal of Aircraft. 37 (6), 1105-1112.

[8] Nissim, E., Gilyard, G.B., 1989. Method for Experimental Determination of Flutter Speed by Parameter Identification. NASA Technical Paper 2923.

[9] Song, J.E., Kim, T., and Song, S.J., Experimental Determination of Unsteady Aerodynamic Coefficients and Flutter Behavior of a Rigid Wing. Journal of Fluids and Structures. 2012, 29:50-61.

[10] Kim, T., System Identification for Coupled Fluid-Structures: Aerodynamics is Aeroelasticity Minus Structure. AIAA Journal, Vol. 49, No. 3, 2011, 503-512.

[11] Roizner, F., Karpel, M., Parametric Flutter Margin Method for Aeroservoelastic Stability Analysis. AIAA Journal, Vol. 56, No. 3, 2017, 1-12.

[12] Kim, T., Surrogate Model Reduction for Linear Dynamic Systems Based on a Frequency Domain Modal Analysis. Computational Mechanics, 2015, 56 (4), 709-723.

[13] Kim, T., Parametric Model Reduction for Aeroelastic Systems: Invariant Aeroelastic Modes, Journal of Fluids and Structures. 2016, 65:196-216.

[14] Kim, T., Flutter Prediction Methodology Based on Dynamic Eigen Decomposition and Frequency-Domain Stability. Journal of Fluids and Structures. 2019, 86:0-13.

[15] Kim, T., Progressive Flutter Prediction Using Flight Data with Limited Actuators and Sensors. AIAA-2024-0194, SciTech 2024, Orlando, FL, January 8-12, 2024.

[16] Dowell, E. H., Thomas, J. P., Hall, K. C., and Denegri C. M., Jr., Theoretical Predictions of F-16 Fighter Limit Cycle Oscillations for Flight Flutter Testing, Journal of Aircraft. 46 (5), 1667-1672.

[17] Zhang, Z., Chen, P.C., Wang, X.Q., and Mignolet, M.P., Nonlinear Aerodynamics and Nonlinear Structures Interaction for F-16 Limit Cycle Oscillation Prediction. AIAA 2016-1796, Jan. 2016.

[18] Denegri, C.M., Dubben, J.A., and Kernazhitskiy, S.L., Underwing Missile Aerodynamic Effects on Flight-Measured Limit-Cycle Oscillations. J. Aircraft. 50 (5), 1637-1645.

[19] Tang, D., Dowell, E.H., and Virgin, L.N., Limit Cycle Behavior of an Airfoil with a Control Surface. Journal of Fluids and Structures. 1998, 12: 839-858.

[20] Maciejowski, J. M., *Multivariable Feedback Design*, Addison Wesley, Longman, Reading, MA, 1989.

[21] Wright, J.R., Wong, J., Cooper, J.E., and Dimitriadis, G., On the Use of Control Surface Excitation in Flutter Testing. Proc. Instn Mech. Engrs Vol. 217 Part G: J. Aerospace Engineering

[22] Meirovitch, L., *Analytical Methods in Vibrations*, Pearson, 1967.

[23] Bisplinghoff, R.L., Ashley, H. and Halfman, H., *Aeroelasticity*, Dover Science, 1996.

COPYRIGHT STATEMENT

The authors confirm that they, and/or their company or organization, hold copyright on all of the original material included in this paper. The authors also confirm that they have obtained permission from the copyright holder of any third-party material included in this paper to publish it as part of their paper. The authors confirm that they give permission or have obtained permission from the copyright holder of this paper, for the publication and public distribution of this paper as part of the IFASD 2024 proceedings or as individual off-prints from the proceedings.